Methodologies for pharmacokinetic post-contrastographic dynamic contrast enhancement

L. Di Paola and A. Fasano

PRABB, Faculty of Biomedical Engineering,
Università Campus Bio-Medico of Rome,
Via Alvaro del Portillo, 21 – 00128, Rome, Italy
E-mail: l.dipaola@unicampus.it
E-mail: a.fasano@unicampus.it

V. Russo*

PRABB, Faculty of Biomedical Engineering,
Università Campus Bio-Medico of Rome,
Via Alvaro del Portillo, 21 – 00128, Rome, Italy
and
DIS, Faculty of System Engineering,
Università Sapienza of Rome,
Via Ariosto, 25 – 00185, Rome, Italy
E-mail: v.russo@unicampus.it
*Corresponding author

R. Setola

PRABB, Faculty of Biomedical Engineering,
Università Campus Bio-Medico of Rome,
Via Alvaro del Portillo, 21 – 00128, Rome, Italy
E-mail: r.setola@unicampus.it

Abstract: Post-contrastographic dynamic contrast enhancement (DCE) technique is a non-invasive method aimed at inquiring the vascularisation induced by lesions; it relies on the analysis of the perfusion's dynamics of contrast agent (CA) within body tissue. The images derived from magnetic resonance (MR), computer tomography (CT) or ultra sound (US) assessments are analysed to derive a contrast enhancement curve, from which some parameters, useful for diagnosis, are acquired. This approach is only qualitative and the estimated parameters have a poor precision and a scarce physical meaning. To overcome these drawbacks, pharmacokinetic models have been introduced for quantitative DCE analysis. In this work, a pharmacokinetic model is proposed, based on physical parameters; it has been applied to the study of post-contrastographic DCE images and parameter estimation has been performed through a maximum likelihood procedure. Results show anomalous value of blood vessel permeability for ill tissues, when compared to healthy ones.

Keywords: biomedical imaging; dynamic contrast enhancement; DCE; pharmacokinetic compartmental modelling; parameter estimation system identification; system modelling.

Reference to this paper should be made as follows: Di Paola, L., Fasano, Russo, V. and A., Setola, R. (2010) 'Methodologies for pharmacokinetic post-contrastographic dynamic contrast enhancement', *Int. J. Modelling, Identification and Control*, Vol. 9, No. 3, pp.267–274.

Biographical notes: Luisa Di Paola received her Master's degree in Chemical Engineering (1997) and her PhD in Industrial Chemical Processing (2001) at the University 'Sapienza' in Rome. She worked (2000), as a Visiting Scholar, at the College of Chemistry – University of California Berkeley, under the supervision of Prof. J.M. Prausnitz and H.W. Blanch. She teaches molecular thermodynamics of biological systems and artificial organs engineering, at the Faculty of Engineering of the University Campus Biomedico. Her main research interests lie in the field of biomedical engineering: artificial organs engineering (oxygenators and bioartificial liver), pharmacokinetic modelling for medical imaging and rheology of complex fluids.

Antonio Fasano received his Laurea degree (summa cum laude) in Electrical Engineering and his PhD in Information and Communications Engineering, both from the University of Rome 'La Sapienza', Rome, Italy, in 1997 and 2001 respectively. Since 2002, he has been with the INFOCOM Dept. of the University of Rome 'La Sapienza', where he held a Postdoctoral position. He has held positions as a Visiting Scientist and a Visiting Professor at the University Campus Bio-Medico, Rome, Italy. In 2007, he joined the University Campus Bio-Medico, where he is a Professor in Biomedical Signal Processing. His primary research interests include information theoretic aspects of MIMO systems, with emphasis on space-time coding and wireless sensor networks.

Valentina Russo received her Master's degree in Computer Science Engineering at the University 'Roma Tre' in Rome (Italy) in the 2006. From 2004, she worked on the development of innovative tools to support the dynamic contrast enhancement analysis cooperating with the Complex System and Security Lab of the University Campus Bio-Medico in Rome. She is a PhD student in System Engineering at University 'La Sapienza' in Rome and she is tutoring automatic control at University Campus Bio-Medico in Rome. Her research interests include development of biomedical systems and automatic image analysis and processing. She is the co-author of four scientific papers.

Roberto Setola received his Laurea degree in Electronic Engineering (1992) and his PhD in Electronic Engineering and Computer Science (1996) from the University of Naples. From 1999 to 2004, he worked at the Italian Prime Minister's Office. At present, he is an Assistant Professor of Automatic Control at University Campus Bio-Medico of Roma and lead of the Complex System and Security Lab. His research interests include modelling and control, control of complex systems, surgery robotics and biomedical systems. He is the author of more than 100 scientific papers.

1 Introduction

Dynamic contrast enhancement (DCE) analysis is one of the most promising techniques for functional medical imaging (Choyke et al., 2003; Jackson, 2004; Lee, 2002; O'Connor et al., 2007; Taylor et al., 1999; Workman et al., 2006, Kirankumar and Shenbaga, 2006, Weon et al., 2006). It is applied for non-invasive analysis of severe lesions, such as inflammatory diseases (Sempere and Sanjuan, 2005; Gourtsoyiannis et al., 2004; Zierhut et al., 2007) and cancer (Rijpkema et al., 2001; Evelhoch, 1999), with an efficacy that is comparable to traditional, more invasive, approaches like histological resections and analysis (Yamashita et al., 2000). DCE has been applied to several studies in the biomedical field, but the main area of application has emerged as oncology, where it is able to support both diagnosis and prognosis. In this regard, though still a hot research topic, DCE analysis is indeed widely applied in clinical practice (Choyke et al., 2003; Jackson, 2004).

The DCE analysis is able to estimate the degree of vascularisation in tissues subject to lesions (Choyke et al., 2003; Jackson, 2004), by analysing the perfusion dynamics of a specific contrast agent (CA) into the body tissues. The DCE analysis is generally arranged in the following way: a specific CA is injected into the body of the patient and several images of a specific region of interest (ROI) are acquired over a time period ranging from 30 seconds to several minutes, depending on the specific analysis carried out. For any image it is defined the contrast enhancement (CE) as:

$$I(t_k, x, y) = \left[i(t_k, x, y) - i_0(x, y) \right] \tag{1}$$

where $i(t_k, x, y)$ denotes the intensity at the spatial position (x, y) of the image acquired at time t_k, whereas $i_0(x, y)$ is the corresponding basal value of the intensity, i.e., the mean value of the measured intensity before the CA injection. The ROI average intensity $I_{ROI}(t_k)$ is evaluated at any time t_k as the average value of the intensity with respect to each pixel in the ROI itself:

$$I_{ROI}(t_k) = \frac{1}{N} \sum_{(x,y) \in ROI} \left[i(t_k, x, y) - i_0(x, y) \right] \tag{2}$$

with N as the number of the pixels within ROI. Moreover, when t_k ranges within the observation interval, the corresponding CE curve $I_{ROI}(t_k)$ is obtained.

DCE analysis can be performed on images produced via ultra sound (US), computer tomography (CT) and magnetic resonance (MR) exams, using specific contrast media; indeed, the last generation top-class US, CT and MR devices integrate dedicated tools intended to perform basic DCE analysis.

Nowadays, DCE analysis is performed by evaluating the CE curve and then determining from it some numerical parameters (Russo et al., 2007; Russo and Setola, 2009). Unfortunately, this approach presents strong limits, since the derived parameters are related solely to the shape of the CE curve and do not provide any information about the physical parameters governing the dynamics of the CA perfusion.

For this reason, in the last years, compartmental pharmacokinetic (PK) models have been arranged, in order to derive more general and valuable information; within this context, the Brix model (Banher et al., 1999) is widely used as a reference to interpret and model DCE data: otherwise, it

is not referring to well established physiological parameters and neglects the whole CA metabolism in body.

In this work, we propose a methodological approach to DCE analysis, based on a PK compartmental model where the physical parameters governing the dynamics of the perfusion phenomenon are explicitly taken into account. In this regard, the main purpose is to derive a set of parameters with physical significance, namely characteristic times that, moreover, can be meaningful from a diagnostic perspective.

Section 2 deals with the application of compartmental models to biomedical imaging and a mathematical model is proposed, with the specific aim of DCE post-contrastographic analysis.

Section 3 is devoted to system model analysis and parameters estimation.

Results are shown in Section 4, with a discussion about some noticeable aspects emerging from the model application.

2 Compartmental models for post-contrastographic DCE

Compartmental modelling provides a powerful framework to represent PK evolution of drugs into body tissues; the main assumption underlying this kind of models is that living bodies may be represented in terms of different compartments, referring to different tissues, whose properties are uniform; thus, every compartment is univocally identified by just one value of a given feature of interest. From a fluidodynamic point of view, any single compartment is then represented as a continuous stirred tank reactor (CSTR) in the case of continuous flow or as a batch stirred tank reactor (BSTR) for closed compartments (Levenspiel, 1999). In the case of post-contrastographic DCE, compartmental modelling relies strongly on the specific type of CA in use: for instance, a small molecular weight compound not only is allowed to move into plasmatic flows or through vascular wall, but could also come into cells, eventually with an uneven distribution.

Many models have been proposed in the literature to describe the time evolution of injected CA into body tissues: a very early class of model, yet still largely applied (Galbraith et al., 2002; Moate et al., 2004; Roberts et al., 2006; Srikanchana et al., 2004), relies on the application of mathematical model for the curve-fitting, whose parameters are just meant to describe experimental data, without physical significance: those models belong to the category of the so-called 'classical PK'.

On the other hand, some other models attempt a physical explanation of parameters they rely on (Bischoff, 1986). The Brix model (Bahner et al., 1999) belongs to this latter class, referred to as 'physiological PK; this model has been used as starting point for the model described in the next paragraph.

For a complete survey of available models for DCE analysis (see Russo and Setola, 2009).

In this work, we dealt only on interstitial, high molecular weight compound: thus, only plasmatic parts of body region are allowed to these molecules, whether within the blood vessels or into the extra-vascular extra-cellular tissue part.

2.1 Open three compartments model

The Brix model (Bahner et al., 1999) considers two compartments: the plasmatic tissue volume and the interstitial, extra-cellular extra-vascular space. In order to improve the fitting capability and the physical description of the model, we introduced into the Brix model some further elements (Figure 1), including

- a systemic blood compartment, describing the general blood mixing and accounting for the incoming flow of the infusion and the CA recycle through the venous flow
- in the systemic blood compartment, a part of the CA is removed by metabolic mechanisms (kidney elimination), with a linear specific rate (for volume unit) $k_M \cdot c_A$.

Figure 1 Open three compartments model

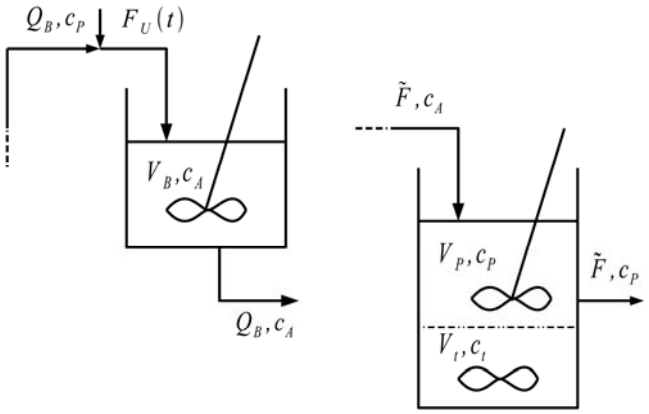

Thus, three compartments are identified: a blood general, a blood regional and a tissue one: the molar outflow coming from the blood general compartment is $Q_B c_A$ and it comes directly to perfuse tissues.

Then our model is composed of a systemic compartment and, for each ROI, we define two compartments:

1 a vascular plasmatic compartment (regional blood flow), fed by the corresponding plasma volumetric flow rate $\tilde{F}$, with a CA concentration c_A; another part of the CA coming from the vascular compartment permeates through the vascular wall and comes into the interstitial extra-cellular tissue, the rate of permeation is $PS \cdot (c_p - c_t)$ where PS is the product of the blood vessel permeability P and S is the overall surface area of blood vessel within the ROI

2 an interstitial, extra-cellular compartment, whose corresponding (uniform) CA concentration is c_t, fed only by the permeation flow $PS \cdot (c_p - c_t)$, coming from the regional plasmatic region.

The corresponding molar balances, for each ROI, are:

- blood systemic flood:

$$V_B \cdot \frac{dc_A}{dt} = Q_B \cdot c_P + F_U(t) - Q_B \cdot c_A - k_R \cdot c_A V_B \tag{3}$$

- blood regional (ROI) flow:

$$V_P \cdot \frac{dc_P}{dt} = \tilde{F} \cdot c_A + \tilde{F} \cdot c_P - PS \cdot (c_P - c_t) \tag{4}$$

- tissue interstitial compartment (ROI):

$$V_t \cdot \frac{dc_t}{dt} = PS \cdot (c_P - c_t) \tag{5}$$

where V_B is the systemic blood volume, V_P is the ROI plasmatic volume and V_t is the ROI interstitial (extra-vascular extra-cellular space) volume.

Equations (3)–(5) may be written such that characteristic times are evidenced, for any kinetic phenomenon (permeation, metabolic removal, residence in each compartment); they are in details defined as follows:

- residence time in the systemic blood compartment (volume V_B):

$$\tau_A = \frac{V_B}{Q_B} \tag{6}$$

- residence time in the ROI blood compartment (volume V_P):

$$\tau_B = \frac{V_P}{\tilde{F}} \tag{7}$$

- permeation time (plasmatic ROI volume V_P):

$$\tau_P = \frac{V_P}{PS} = \frac{1}{Pa} \tag{8}$$

where $a = \frac{S}{V_P}$ is the specific surface area of blood vessel, per unit volume of the plasmatic ROI part V_P

- metabolic removal time (systemic blood volume V_B):

$$\tau_M = \frac{1}{k_R} \tag{9}$$

Mass balances then become:

$$\frac{dc_A}{dt} = -c_A \cdot \left[\frac{1}{\tau_A} + \frac{1}{\tau_M}\right] + \frac{c_P}{\tau_A} + \frac{F_U(t)}{V_B} \tag{10}$$

$$\frac{dc_P}{dt} = \frac{c_A}{\tau_B} - \left[\frac{1}{\tau_B} + \frac{1}{\tau_M}\right] \cdot c_P + \frac{1}{\tau_P} c_t \tag{11}$$

$$\frac{dc_t}{dt} = \frac{\alpha_P}{\tau_P}(c_P - c_t) \tag{12}$$

Equations (10)–(12) vary due to the different infusion function $F_U(t)$. In the case of continuous infusion, the input infusion function is:

$$F_U(t) = Q_I \cdot c_I \tag{13}$$

where Q_I is the infusion flow rate and c_I is the corresponding CA concentration.

2.2 Intensity-concentration conversion

In order to set-up a quantitative relation between intensity variation measured in each compartment with the corresponding CA concentration, we should introduce a calibration factor β, defined as:

$$I = \beta \cdot c \tag{14}$$

where I is the enhanced intensity without the observation noise and c is the CA concentration. Equation (14) relies on the hypothesis, widely accepted as reliable, that the measured intensity is directly proportional to the corresponding local CA concentration.

In the literature, the calibration factor is generally considered as a known factor, but unfortunately, in the clinical practice, this is not the case. As a consequence, we assume β to be an additional unknown parameter that can be estimated following the procedure described in the next section. However, it is worth noting that the knowledge of an estimate of β is not particularly significant from a diagnostic perspective, since the interesting parameters in this regard are the characteristic times defined previously.

Besides the calibration factor, we need to establish the relation between the concentrations introduced in the compartmental model and the enhanced intensities corresponding to the specific ROI. In this regard, it is useful to observe that the number of moles of the CA in the ROI, denoted by n_{ROI}, is given as a sum of two contributes: the number of moles in the interstitial space n_t and in the plasmatic ROI part n_P:

$$n_{ROI} = n_t + n_P \tag{15}$$

and, in terms of concentrations:

$$V_{ROI} \cdot c_{ROI} = V_t \cdot c_t + V_P \cdot c_P \tag{16}$$

where $V_{ROI} = V_t + V_P$ (in the case of interest of an interstitial CA, it does not come into the cells); thus, in terms of concentrations:

$$c_{ROI} = \frac{1}{1+\alpha_P} \cdot c_t + \frac{\alpha_P}{1+\alpha_P} \cdot c_P \tag{17}$$

which is the relation that will be used in the next section to settle the observation model.

3 System model and parameters estimation

The compartmental model introduced in the previous section, can be recast in terms of a dynamic system whose state is composed of the concentration functions in the three compartments there defined. The dynamic matrix of the system is determined by the differential equations (10), (11) and (12), which govern the corresponding mass balances.

Moreover, the input is the unit step function since we considered the case of continuous infusion of the CA. The system is:

$$\begin{cases} x(t) = \boldsymbol{A}x(t) + \boldsymbol{b}u(t) \\ x(0) = 0 \end{cases} \tag{18}$$

where $u(t)$ is the unit step function, the state vector $x(t)$ gathers the concentration functions in the three compartments:

$$\boldsymbol{x}(t) = \begin{bmatrix} c_A(t) \\ c_P(t) \\ c_t(t) \end{bmatrix} \tag{19}$$

and the dynamic matrix $\boldsymbol{A}$ and the vector $\boldsymbol{b}$ are defined as

$$\boldsymbol{A} = \begin{bmatrix} -\left(\frac{1}{\tau_A} + \frac{1}{\tau_M}\right) & \frac{1}{\tau_A} & 0 \\ \frac{1}{\tau_B} & -\left(\frac{1}{\tau_B} + \frac{1}{\tau_P}\right) & \frac{1}{\tau_P} \\ 0 & \frac{\alpha_P}{\tau_P} & -\frac{\alpha_P}{\tau_P} \end{bmatrix} \tag{20}$$

$$\boldsymbol{b} = \begin{bmatrix} \frac{Q_I c_I}{V_B} \\ 0 \\ 0 \end{bmatrix} \tag{21}$$

respectively.

The dynamic matrix $\boldsymbol{A}$ depends on the unknown physical parameters, namely, τ_A, τ_B, τ_M, τ_P, α_P, which will be subsequently estimated in order to identify the system. To this purpose, and for the sake of compactness in the notation, we introduce the following vector which gathers all the parameters associated with the compartmental model and moreover includes the calibration factor β.

$$\boldsymbol{\theta} = \left[\tau_A \ \tau_B \ \tau_M \ \tau_P \ \alpha_P \ \beta\right]^T \tag{22}$$

We model $\boldsymbol{\theta}$ as a vector of unknown, i.e., not random, parameters. This choice is motivated by the fact that it is not available in the open literature any information about the statistics of $\boldsymbol{\theta}$ or any of its components. As a consequence, $\boldsymbol{\theta}$ will be estimated resorting to the maximum likelihood criterion.

Now, let us analyse the properties of the matrix $\boldsymbol{A}$ since they affect the solutions of system. By hypothesis, the parameters defining $\boldsymbol{A}$ are strictly positive and this condition combined with the structure of $\boldsymbol{A}$ entails a useful property of this matrix, which is summarised in the following.

Proposition 1: The matrix $\boldsymbol{A}$ in (1.20) has only negative real eigenvalues, for any positive value of the parameters τ_A, τ_B, τ_M, τ_P, α_P.

Proof: The matrix $\boldsymbol{A}$ is diagonally dominant (Horn and Johnson, 1985) with negative diagonal entries and this implies, exploiting the Geršgorin disc theorem (Horn and Johnson, 1985), that all its non-null eigenvalues have negative real part. Moreover, zero is not an eigenvalue of $\boldsymbol{A}$ since $\det(\boldsymbol{A}) = -\frac{\alpha_P}{\tau_B \tau_M \tau_P} \neq 0$. It remains to prove that $\boldsymbol{A}$ has only real eigenvalues. This is indeed the case since $\boldsymbol{A}$ is tridiagonal and its entries, denoted by $a_{k,j}$, satisfy the following conditions

$$a_{i,i+1} \cdot a_{i+1,i} \geq 0 \text{ for } i = 1, 2, 3$$

This is sufficient (Horn and Johnson, 1985) to guarantee that $\boldsymbol{A}$ is similar to a symmetric matrix, and thus has only real eigenvalues. Finally, these properties hold true regardless of the value of the parameters that define $\boldsymbol{A}$, as long as they are positive, and this proves the claim.

It is worth noting the importance of Proposition 1. Indeed, it guarantees not only that the system (1.18) is asymptotically stable, but also that the evolution of the state, which corresponds to the evolution of the concentrations in the compartmental model, does not contain oscillating terms, possibly dumped. In this regard, our model is consistent with the physical evidence that confirms such behaviour.

Since $\boldsymbol{A}$ is invertible, the solution to (1.18) can be easily determined as

$$\begin{aligned} \boldsymbol{x}(t;\boldsymbol{\theta}) &= e^{\boldsymbol{A}t}\boldsymbol{x}(0) + \int_0^t e^{\boldsymbol{A}(t-\xi)}\boldsymbol{b}u(\xi)\,d\xi \\ &= \boldsymbol{A}^{-1}\left(e^{\boldsymbol{A}t} - \boldsymbol{I}\right)\boldsymbol{b} \quad t \geq 0 \end{aligned}$$

where in the last equality, we have exploited the commutativity of $e^{\boldsymbol{A}t}$ and $\boldsymbol{A}^{-1}$, and we have explicitly indicated the dependence of the solution on the vector of unknown parameters $\boldsymbol{\theta}$.

The whole state vector $x(t, \boldsymbol{\theta})$ is in general inaccessible, but some of its components can be measured, indirectly and through a noisy observation, from the evaluation of the corresponding CE curve. This last can be obtained following the acquisition scheme described in the previous sections. To this purpose, we assume the availability of M images, which correspond to the same section of the patient's body under analysis, taken at $0 = t_1 < t_2 < \ldots < t_M$.

Then, from every image we select the same set of ROIs[1] and for each ROI, within each single image, we compute the sample of the corresponding CE curve. Let us denote by $\boldsymbol{y}_k$ the column vector gathering the different samples of the CE curves computed at time t_k from the different ROIs selected within the k-th image. Thus, we assume that the following observation model is valid for $k = 1, \ldots, M$.

$$\boldsymbol{y}_k = \boldsymbol{C}(\boldsymbol{\theta})\,\boldsymbol{x}(t_k;\boldsymbol{\theta}) + \boldsymbol{w}_k \tag{23}$$

where $\boldsymbol{C}(\boldsymbol{\theta})$, in accordance with (14) and (21), is a matrix with the following structure

$$\boldsymbol{C}(\boldsymbol{\theta}) = \beta \begin{bmatrix} 1 & 0 & 0 \\ 0 & \dfrac{\alpha_P}{1+\alpha_P} & \dfrac{1}{1+\alpha_P} \end{bmatrix}$$

with β being the calibration factor defined in the previous section. We have explicitly considered the case of two ROIs within each image: one related to the systemic blood compartment and the other to the tissue under examination. The term $\boldsymbol{w}_k$ in (23) is a two-dimensional Gaussian random vector sequence with zero mean and autocorrelation function $\mathrm{E}\left\{\boldsymbol{w}_j \boldsymbol{w}_k^T\right\} = \delta_{j,k}\sigma^2 I_2$, where $\delta_{j,k}$ is the Kronecker delta and $\boldsymbol{I}_2$ is the 2 × 2 identity matrix. As a consequence, in our model the noise affecting the samples of the CE curves are composed of i.i.d.[2] zero mean Gaussian random variables with the same variance. With respect to the validity of this assumption it is worth pointing out some remarks. It should be noted that, in general, the statistics of the noise affecting the value of the pixels of an image cannot be assumed Gaussian, because the noise itself is a combination of several contributes, among which there is the quantisation noise, which is not Gaussian. However the Gaussianity of $\boldsymbol{w}_k$ in (23) can be justified by invoking the central limit theorem, since the computation of the CE curves involves averaging operations carried out over many different pixels. For the same reason, namely averaging operations, the variances of the noise samples can be assumed equal.

Now, let us consider (23) for k = 1, ..., N and introduce the following vectors

$$\boldsymbol{Y} = \begin{bmatrix} \boldsymbol{y}_1 \\ \boldsymbol{y}_2 \\ \vdots \\ \boldsymbol{y}_M \end{bmatrix} \quad \boldsymbol{X}(\boldsymbol{\theta}) = \begin{bmatrix} \boldsymbol{x}(t_1;\boldsymbol{\theta}) \\ \boldsymbol{x}(t_2;\boldsymbol{\theta}) \\ \vdots \\ \boldsymbol{x}(t_M;\boldsymbol{\theta}) \end{bmatrix} \quad \boldsymbol{W} = \begin{bmatrix} \boldsymbol{w}_1 \\ \boldsymbol{w}_2 \\ \vdots \\ \boldsymbol{w}_M \end{bmatrix}$$

then the observation model can be recast into the following compact notation

$$\boldsymbol{Y} = \left[\boldsymbol{I}_M \otimes \boldsymbol{C}(\boldsymbol{\theta})\right]\boldsymbol{X}(\boldsymbol{\theta}) + \boldsymbol{W} \tag{24}$$

where ⊗ denotes the Kronecker product and $\boldsymbol{I}_M$ is the $M \times M$ identity matrix. Moreover, $\boldsymbol{W}$ is a $2M$-sized Gaussian random vector with zero mean and covariance matrix $\mathrm{E}\left\{\boldsymbol{W}\boldsymbol{W}^T\right\} = \sigma^2 \boldsymbol{I}_{2M}$.

Since $\boldsymbol{\theta}$ has been assumed non-random, $\boldsymbol{Y}$ is a Gaussian random vector with mean vector $\mathrm{E}\{\boldsymbol{Y}\} = \left[\boldsymbol{I}_M \otimes \boldsymbol{C}(\boldsymbol{\theta})\right]\boldsymbol{X}(\boldsymbol{\theta})$ and covariance matrix the same as $\boldsymbol{W}$. Thus, its probability density function is given by the following expression

$$p_{\boldsymbol{Y};\boldsymbol{\theta}}(\boldsymbol{Y};\boldsymbol{\theta}) = \frac{1}{\left(2\pi\sigma^2\right)^M} e^{-\frac{1}{2\sigma^2}\left\|\boldsymbol{Y}-(\boldsymbol{I}_M \otimes \boldsymbol{C})\boldsymbol{X}(\boldsymbol{\theta})\right\|^2} \tag{25}$$

that will be subsequently used for the estimation of $\boldsymbol{\theta}$.

3.1 Parameters estimation

Since $\boldsymbol{\theta}$ has been assumed non-random, we estimate it following the maximum likelihood approach (Kay, 1993). From the observation model (24) we have already derived in (25) the probability density function of $\boldsymbol{W}$ dependant on $\boldsymbol{\theta}$. From (25) the corresponding log-likelihood function is computed

$$\begin{aligned} L(\boldsymbol{\theta}) &= \log[p(Y,\boldsymbol{\theta})] \\ &= -\frac{1}{2\sigma^2}\left\|Y - [I_M \otimes C(\boldsymbol{\theta})]X(\boldsymbol{\theta})\right\|^2 - M\log(2\pi\sigma^2) \end{aligned}$$

and the maximum likelihood estimate of $\boldsymbol{\theta}$ is determined solving the following optimisation problem

$$\begin{aligned} \hat{\boldsymbol{\theta}}(Y) &= \arg\max_{\theta} L(\boldsymbol{\theta}) \\ &= \arg\min_{\boldsymbol{\theta}} \left\|Y - [I_M \otimes C(\boldsymbol{\theta})]X(\boldsymbol{\theta})\right\|^2 \\ &= \arg\min_{\boldsymbol{\theta}} \sum_{k=1}^{M} \left\|y_k - C(\boldsymbol{\theta})x(t_k,\boldsymbol{\theta})\right\|^2 \end{aligned} \tag{26}$$

where all the terms have been previously defined. It is interesting to note that in this case, due to the fact that the noise samples affecting the observed data have been assumed i.i.d. Gaussian random variables, the maximum likelihood estimation amounts to solving a non-linear least square problem. The minimisation problem in (26) has been solved numerically.

4 Results and discussion

Clinical images acquisition over time was performed via Siemens MR on axial plane, with a positive step intravenous administration of the contrast media, during the whole test (images are kindly provided by the Department of Imaging, Faculty of Medicine, Università Campus Bio-Medico of Rome, Italy).

Model has been applied to clinical images, referred to Chron's disease, i.e., an inflammatory disease due to an autoimmune disorder of unknown origin that affects mainly young people, with a chronic and relapsing course.

In Figure 2, results of the model application to clinical data are shown, normalised with respect to the asymptotic value of CA aortic concentration.

As it can be seen, the model is in good accordance with the clinical data and estimated model parameters are listed in the table below, for disease at different degrees of morbidity (Table 1).

It is evidenced that in the case of active disease, the difference between the c_A and c_{ROI} is limited, that indicates a large vascularisation of the tissue. As derived from the corresponding parameters in table, in the case of Crohn's disease, the anomalous vascularisation of the tissue corresponds to a larger volumetric fraction of the plasmatic part of the ROI, with respect to negative (sane) tissue, yet with comparable permeation time values.

Figure 2 Crohn's active case

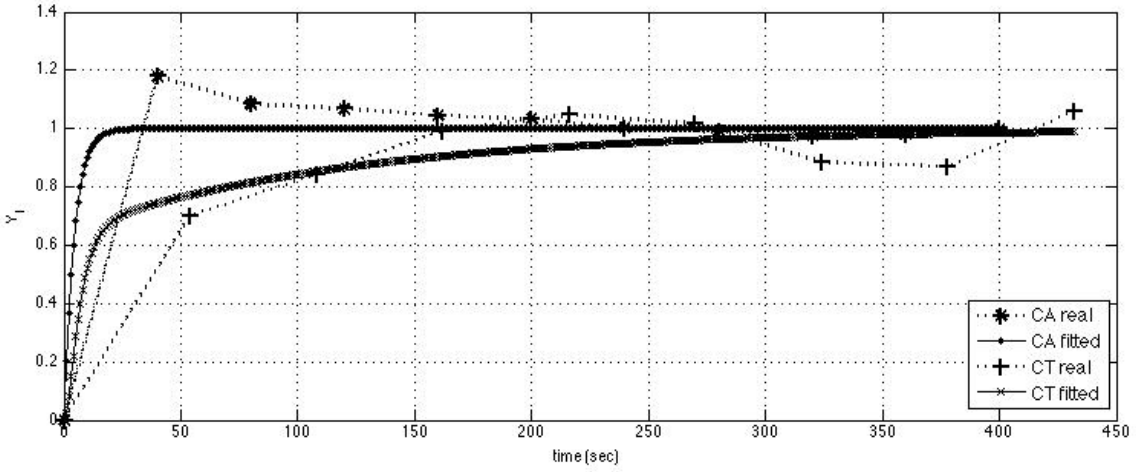

Notes: Real data (dotted line) and fitted data (solid line).

Table 1 Model parameters as derived from clinical data fitting

	τ_A, [S]	τ_M, [S]	τ_B, [S]	τ_P, [S]	α_P
Inactive (case 1)	83,1898	4,3545	0,0083	266,3231	0,5541
Inactive (case 2)	86,9938	4,1619	0,0027	266,4191	0,6113
Active	87,8719	4.9816	2,1498	251,6900	2,0628
Negative	80,8079	6,9968	0,8147	262,3221	0,1686

On the other hand, the systemic values of τ_A and τ_M are very similar, for every case, to each others, which indicate that the model is consistent in describing the local anomalies, without interfering on global parameters.

5 Conclusions

In this work, a new methodological approach is proposed for DCE imaging analysis, in the path moving from empirical CE curve study to physically PK modelling.

The described methods have shown two features: they are simple to apply, in some given conditions (continuous CA infusion) and they permit to derive some parameters with a specific physical meaning. These values can be used as diagnostic tools, with the ultimate goal to provide a procedure no more relying on histopathological invasive analysis methods.

Even though with the wide limitations introduced with the model hypothesis, the model appears to be suitable to the description of DCE imaging. We are working on some improvements, especially regarding the introduction of a delay to describe more properly the input arterial function c_A^{∞}.

The improvement obtained with the introduction of the concentration curves in contrast to the enhancement curves relies on the objectivity of the diagnosed. All the values are referred to the maximum concentration value: the arterial concentration curve, which value is normalised to 1. It is simple, in this way, to compare different patients even if they present different physiological characteristics and/or their exams were derived from different protocols and scanner.

References

Bahner, M.L., Brix, G., Hoffmann, U., Horvath, A. and Schreiber, W. (1999) 'Regional blood flow, capillary permeability and compartmental volumes: measurement with dynamic CT-initial experience', *Radiol*, Vol. 210, pp.269–276.

Bischoff, K. (1986) 'Physiological pharmacokinetics', *Bull Math Biol*, Vol. 48, No. 3, pp.309–322.

Choyke, P., Dwyer, A. and Knopp, M. (2003) 'Functional tumor imaging with dynamic contrast-enhanced magnetic resonance imaging', *J Magn Reson Imaging*, Vol. 17, No. 5, pp.509–520.

Evelhoch, J. (1999) 'Key factors in the acquisition of contrast kinetic data for oncology', *J Magn Reson Imaging*, Vol. 10, pp.254–259.

Galbraith, S., Lodge, M., Taylor, N., Rustin, G., Bentzen, S., Stirling, J. and Padhani, A. (2002) 'Reproducibility of dynamic contrast-enhanced MRI in human muscle and tumours: comparison of quantitative and semi-quantitative analysis', *NMR Biomed*, Vol. 15, No. 2, pp.132–142.

Gourtsoyiannis, N., Papanikolaou, N., Grammatikakis, J., Papamastorakis, G., Prassopoulos, P. and Roussomoustakaki, M. (2004) 'Assessment of Crohn's disease activity in the small bowel with MR and conventional enteroclysis: preliminary results', *Eur Radiol*, Vol. 14, No. 6, pp.1017–1024.

Horn, R. and Johnson, C. (1985) *Matrix Analysis*, Cambridge University Press.

Jackson, A. (2004) 'Analysis of dynamic contrast enhanced MRI', *Brit J Radiol*, Vol. 77, Special Issue 2, pp.S154–166.

Kay, S.M. (1993) *Fundamentals of Statistical Signal Processing: Estimation Theory, Volume 1*, Prentice Hall PTR.

Kirankumar, Y. and Shenbaga, D.S. (2007) 'Transform-based medical image fusion', *Int J Biomed Eng Tech*, Vol. 1, No. 1, pp.101–110.

Lee, T. (2002) 'Functional ct: physiological models', *Trends Biotechnol*, Vol. 20, No. 8, pp.3–10.

Levenspiel, O. (1999) *Chemical Reaction Engineering*, Wiley.

Moate, P., Dougherty, L., Schnall, M., Landis, R. and Boston, R. (2004) 'A modified logistic model to describe gadolinium kinetics in breast tumors', *Magn Reson Med*, Vol. 22, No. 4, pp.467–473.

O'Connor, J., Jackson, A., Parker, G. and Jayson, G. (2007) 'DCE-MRI biomarkers in the clinical evaluation of antiangiogenic and vascular disrupting agents', *Br J Cancer*, Vol. 96, pp.189–195.

Rijpkema, M., Kaanders, J., Joosten, F., van der Kogel, A. and Heerschap, A. (2001) 'Method for quantitative mapping of dynamic MRI contrast agent uptake in human tumors', *J Magn Reson Imaging*, Vol. 14, No. 4, pp.457–463.

Roberts, C., Issa, B., Stone, A., Jackson, A., Waterton, J.C. and Parker, G.J.M. (2006) 'Comparative study into the robustness of compartmental modeling and model-free analysis in DCE-MRI studies', *J Magn Reson Imaging: JMRI*, Vol. 23, No. 4, pp.554–563.

Russo, V. and Setola, R. (2009) 'Dynamic contrast enhancement: analysis's models and methodologies', *Handbook of Research on Advanced Techniques in Diagnostic Imaging and Biomedical Applications*, IGI Global.

Russo, V., Setola, R., Vescovo, R.D., Grasso, R. and Zobel, B.B. (2007) 'DyCoH: an innovative tool to dynamic contrast enhancement analysis', *Engineering in Medicine and Biology Society. 29th Annual International Conference of the IEEE*, p.63.

Sempere, G. and Sanjuan, M. (2005) 'MRI evaluation of inflammatory activity in Crohn's disease', *Am J Roentgenol*, Vol. 184, No. 6, pp.1829–1835.

Srikanchana, R., Thomasson, D., Choyke, P. and Dwyer, A. (2004) 'A comparison of pharmacokinetic models of dynamic contrast enhanced MRI in computer-based medical systems', *Proceedings on 17th IEEE Symposium*, pp.361–366.

Taylor, J., Tofts, P., Port, R., Evelhoch, J., Knopp, M., Reddick, W., Runge, V. and Mayr, N. (1999) 'MR imaging of tumor microcirculation: promise for the new millenium', *Magn Reson Med*, Vol. 10, pp.903–907.

Weon, B.M., Je, J.H., Hwu, Y. and Margaritondo, G. (2006) 'Phase contrast X-ray imaging', *Int J Nanotechnology*, Vol. 3 Nos. 2/3, pp.280–297.

Workman, P., Aboagye, E., Chung, Y., Griffiths, J., Hart, R., Leach, M., Maxwell, R., McSheehy, P., Price, P. and Zweit, J. (2006) 'Minimally invasive pharmacokinetic and pharmacodynamic technologies in hypothesis-testing clinical trials of innovative therapies', *J Natl Cancer Inst*, Vol. 98, No. 9, pp.580–598.

Yamashita, Y., Baba, T., Baba, Y., Nishimura, R., Ikeda, S., Takahashi, M., Ohtake, H. and Okamura, H. (2000) 'Dynamic contrast-enhanced MR imaging of uterine cervical cancer: pharmacokinetic analysis with histopathologic correlation and its importance in predicting the outcome of radiation therapy', *Radiol*, Vol. 216, No. 3, pp.803–809.

Zierhut, M.L., Gardner, J.C., Spilker, M.E., Sharp, J.T. and Vicini, P. (2007) 'Kinetic modeling of contrast-enhanced MRI: an automated technique for assessing inflammation in the rheumatoid arthritis wrist', *Ann Biomed Eng*, Vol. 35, No. 5, pp.781–795.

Notes

1 In general we extract several CE curves from the same set of images.

2 Independent identically distributed.